How to tell a gravastar from a black hole

Cecilia B M H Chirenti[1,2] **and Luciano Rezzolla**[2,3]

[1] Instituto de Física, Universidade de São Paulo, São Paulo, Brazil
[2] Max-Planck-Institut für Gravitationsphysik, Albert Einstein Institut, 14476 Golm, Germany
[3] Department of Physics, Louisiana State University, Baton Rouge, LA 70803 USA

Abstract. Gravastars have been recently proposed as potential alternatives to explain the astrophysical phenomenology traditionally associated to black holes, raising the question of whether the two objects can be distinguished at all. Leaving aside the debate about the processes that would lead to the formation of a gravastar and the astronomical evidence in their support, we here address two basic questions: Is a gravastar stable against generic perturbations? If stable, can an observer distinguish it from a black hole of the same mass? To answer these questions we construct a general class of gravastars and determine the conditions they must satisfy in order to exist as equilibrium solutions of the Einstein equations. For such models we perform a systematic stability analysis against axial-perturbations, computing the real and imaginary parts of the eigenfrequencies. Overall, we find that gravastars are stable to axial perturbations, but also that their quasi-normal modes differ from those of a black hole of the same mass and thus can be used to discern, beyond dispute, a gravastar from a black hole.

1. Introduction

The gravastar model was proposed by Mazur and Mottola [1] and has attracted attention as a possible alternative to black holes. Within this model, in fact, a massive star in its late stages could end its life as a gravastar, namely a very compact object whose radius would be very close to the Schwarzschild radius (indeed arbitrarily close to it) without having an event horizon or a central singularity. For this to happen, a phase transition is expected to take place at or near the location where the event horizon would have been formed otherwise [2]. The interior of what would have been the black hole is replaced by a suitably chosen portion of de-Sitter spacetime with an equation of state (EOS) $p = -\rho$, surrounded by a thin shell of ultra-stiff matter with EOS $p = +\rho$, and which is then suitably matched to a Schwarzschild vacuum. In practice, the Mazur-Mottola gravastar model, hereafter the MM model [1], is a spherically symmetric and static five-layer solution of the Einstein equations, including two infinitesimally thin shells needed by the junction conditions of the metric [3].

For as much as it is ingenious, the gravastar model also challenges a building block in modern astronomy, namely the existence of astrophysical black holes. In spite of the many observational evidences in favour of black holes, it may indeed be fundamentally impossible to give an irrefutable observational proof for the existence of a black-hole horizon if only electromagnetic radiation is received [4] and thus tell apart a black hole from a gravastar, if the latter existed. Such a challenge has obviously attracted a lot of attention and several related models have been recently proposed in the attempt of providing answers to two basic questions: Once produced, is a gravastar stable to generic perturbations? If stable, can an external obverver distinguish a gravastar from a black hole of the same mass?

In ref. [1] it was argued that the MM solution is thermodynamically stable, but other stability analysis are not so easy to perform because of the model's structure. Visser and Wiltshire [5] have analyzed the radial stability of a simplified model with three layers and the stability was shown to hold for a number of configurations. This stability was generalized by Carter [6] for gravastar models with different exteriors. Other possibilities for the interior solution have also been considered: Bilić *et al* [7] replaced the de-Sitter interior by a Born-Infeld phantom, while Lobo replaced the interior solution by one that is governed by the dark-energy EOS [8], and Lobo and Arellano matched interior nonlinear electrodynamic geometries to the Schwarzschild exterior [9].

To remove in part the complications produced by the infinitesimal shells in the MM model, Cattoen *et al* [10] have found that fluid gravastars can be built if the fluid is confined to a given layer and has there anisotropic pressures. The latter essentially replace the surface tension which was introduced in the original model MM model by the matching of the metric in the infinitesimally thin shells. Although anisotropic and with rather arbitrary equations of state, these pressures have the appealing property of being continuous and thus of allowing one to build equilibrium models without the presence of infinitesimally thin shells and thus look more seriously into the issue of stability. Indeed, as a step to go beyond the construction of equilibrium models, DeBenedictis *et al* [11] made a first attempt to investigate the stability of gravastars through a qualitative analysis of axial perturbations.

In order to provide more definitive answers to the questions mentioned above, we have constructed a general class of fluid gravastars with finite shell thickness and variable compactness. While this class is similar and has been inspired by the one proposed in [10, 11], it also differs in two important aspects. Firstly, while we also consider a fluid gravastar with anisotropic pressures, we try and reproduce the most salient features of the original MM model by creating an internal and an external region which reproduce a de-Sitter and a Schwarzschild spacetime at finite radii and not only asymptotically. Secondly, for these models we determine

precise bounds for the properties of the metric functions and the compactness of the gravastar that yield equilibrium solutions, thus restricting considerably the class of possible solutions.

Using these models we have carried out a systematic investigation of the stability analysis of gravastars against axial-perturbations [12, 13], thus extending the results discussed in [14] to our gravastar model and computing explicit eigenfrequencies. In this way we were able to conclude that: a gravastar *is stable* to axial perturbations and indeed *it is possible* to distinguish it from a black hole if gravitational radiation is produced. More specifically, we have found that for all the models considered the imaginary part of the eigenfrequencies is always negative, thus indicating stability against these perturbations. Furthermore, while it is always possible to build a gravastar with given compactness and thickness such that it will have the same oscillation frequency as that of a black hole with the same mass, the corresponding decaying time will be different. Our results thus provide a way of distinguishing observationally and beyond dispute a gravastar from a black hole.

The paper is organized as follows: in section 2 we review the main features of the original MM model and obtain numerical solutions which enable us to impose bounds for the parameters of the MM solution. In section 3, instead, we present our model for a fluid gravastar with anisotropic pressures and discuss the bounds derived from general conditions imposed by the EOS and the properties of the metric functions. In Section 4 we outline the perturbation equations and the numerical methods employed in the study of axial perturbations of our model. In section 5 we discuss the results obtained for the QNMs and in section 6 we present our final conclusions.

2. The MM gravastar model

We first present a quick review on the main features of the original MM model [1] for they will be used in further developments in this paper and highlight that precise bounds exist for the existence of solutions even for the simplest gravastar model.

In general, we consider a static and spherically symmetric line element

$$ds^2 = -f(r)dt^2 + \frac{dr^2}{h(r)} + r^2 d\Omega^2 \,, \tag{1}$$

and the Einstein equations must be solved for a perfect fluid at rest, such that there are three different regions with the three different equations of state

$$
\begin{array}{llll}
\text{I.} & \text{Interior:} & 0 \le r \le r_1 \,, & \rho = -p \,, \\[6pt]
\text{II.} & \text{Shell:} & r_1 \le r \le r_2 \,, & \rho = +p \,, \\[6pt]
\text{III.} & \text{Exterior:} & r_2 \le r \,, & \rho = p = 0 \,.
\end{array}
\tag{2}
$$

In region I, ρ is a constant given by $\rho_v = 3H_0^2/8\pi$, and the metric is that of a de-Sitter spacetime, so

$$f(r) = Ch(r) = C(1 - H_0^2 r^2) \,, \qquad 0 \le r \le r_1 \,. \tag{3}$$

where C is an integration constant, whose value will be determined later [*cf.* eq. (8)].

In region II, a new dimensionless variable w is defined as $w \equiv 8\pi r^2 p$, in order to obtain the following set of equations

$$\frac{dr}{r} = \frac{dh}{1 - w - h} \,, \tag{4}$$

$$\frac{\mathrm{d}h}{h} = -\left(\frac{1-w-h}{1+w-3h}\right)\frac{\mathrm{d}w}{w}\,, \tag{5}$$

$$\frac{wf}{r^2} = \mathrm{const.} \tag{6}$$

An analytical solution can be obtained in the case of a very thin shell, *i.e.*, for $r_1 \to r_2$. It is easy to see that (4) is satisfied if we take $h = 1 - \bar{m}/r$ and $\mathrm{d}\bar{m}(r) = 2\mathrm{d}m(r) = 8\pi\rho r^2 \mathrm{d}r^2 = w\mathrm{d}r$. Therefore, in the thin-shell limit, (4) can be integrated to yield

$$h \equiv 1 - \frac{\bar{m}}{r} \simeq \epsilon\frac{(1+w)^2}{w} \ll 1\,, \tag{7}$$

where ϵ is an integration constant. From the continuity of the metric coefficients f and h at r_1 and r_2, it can be shown that the integration constants ϵ, C, M and H_0 are given in terms of r_1, r_2, w_1 and w_2 by the relations

$$\epsilon = -\ln\frac{r_2}{r_1}\left(\ln\frac{w_2}{w_1} - \frac{1}{w_2} + \frac{1}{w_1}\right)^{-1}\,, \tag{8}$$

$$C = \left(\frac{1+w_2}{1+w_1}\right)^2\,, \tag{9}$$

$$M = \frac{r_2}{2}\left[1 - \frac{\epsilon(1+w_2)^2}{w_2}\right] = m(r_2)\,, \tag{10}$$

$$H_0^2 = \frac{1}{r_1^2}\left[1 - \frac{\epsilon(1+w_1)^2}{w_1}\right]\,. \tag{11}$$

Finally, in region III and because of Birkhoff's theorem, the spacetime is described by the Schwarzschild metric,

$$f(r) = h(r) = 1 - \frac{2M}{r}\,, \qquad r_2 \le r\,. \tag{12}$$

Clearly, region II is the most interesting one from a physical point of view since it is where a non-trivial model for the gravastar can be specified. In the case of a "thick shell", that is away from the thin-shell limit, the gravastar solution in region II can be obtained in the same way as for ordinary spherical stars, namely through the numerical solution of the Tolman-Oppenheimer-Volkoff (TOV) equations for $\rho(r) = p(r)$ and $m(r)$. We recall that in the MM model $\rho(r)$ and $p(r)$ are discontinuous in r_1 and r_2 and that $m(r_1)$ must, of course, be less than $r_1/2$

By specifying r_1, r_2, and thus the shell thickness $\delta \equiv r_2 - r_1$, as well as the initial conditions for the pressure $p(r_1)$ and mass $m(r_1)$, the numerical solution of the TOV equations provides $m(r)$ and $\rho(r)$ for $r_1 < r \le r_2$. A systematic analysis has revealed that a limit exists on the compactness $\mu \equiv M/r_2$ of the gravastar and in particular that, for given r_1, r_2 and $m(r_1)$ very close to the limit $r_1/2$, there exists a value for $\rho(r_1)$ which provides the largest M. In other words, it is not possible to achieve arbitrary values for M. On the other hand, if we fix r_2 and decrease r_1 so as to increase the thickness of the shell, we must also decrease $m(r_1)$, and we have verified that the maximum value obtained for M also decreases. Overall, therefore, each shell thickness δ also selects a maximum compactness of the gravastar μ, above which no solution of the TOV equations can be found.

All of this is shown in figure 1 which reports the space of parameters (δ, μ) where equilibrium solutions can be found. The solid curve, in particular, is computed numerically and distinguishes the region where equilibrium models can be found (*i.e.*, the region below the curve), from the region where no solutions can be found (*i.e.*, the region above the curve). Stated differently, for any given shell thickness δ, the solid curve marks the

maximum compactness (*i.e.*, the largest value of μ) for which gravastar models can be built. Interestingly, therefore, it is not possible to build a very compact gravastar with a very thick matter shell. Rather, gravastars have either large compactness and thin shells, or small compactness and thicker shells, as shown in figure 1. This figure, and its inset in particular, also illustrates that gravastars can be built with arbitrarily large compactness, *i.e.*, with $\mu \to 1/2$ and thus with the outer radius r_2 being only infinitesimally larger than the corresponding Schwarzschild radius. It is exactly this property that makes gravastars hard to distinguish from a black hole if only electromagnetic radiation is available.
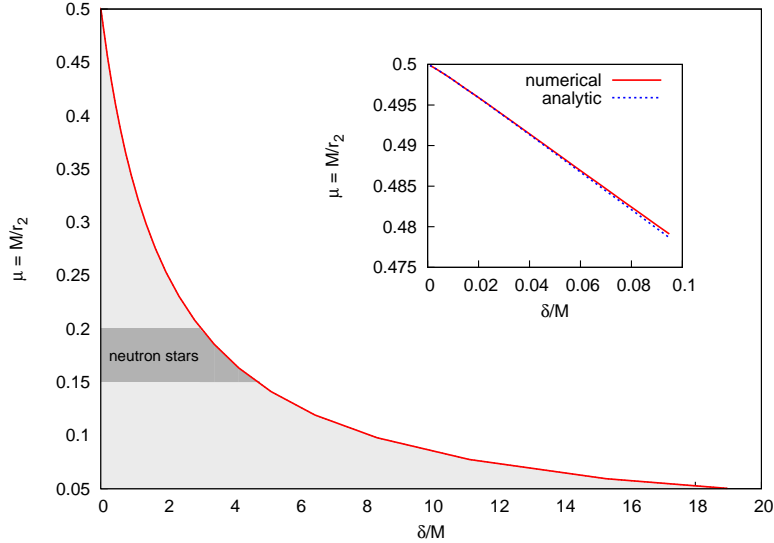

Figure 1. Limits in the compactness and thickness of a gravastar in the MM model. The curve shows the maximum compactness for a given thickness δ of the shell, that is, in the light gray area below the curve we have the possible solutions, while in the area above the curve solutions are no longer possible. The dark gray area highlights the typical compactnesses for neutron stars. The inset shows a comparison between the numerical solution of the TOV equations with the analytical solution in the thin-shell limit.

3. The gravastar model with anisotropic pressures

3.1. The field equations

We now discuss our suggestion for a fluid gravastar model in which we follow the spirit of the original MM model and consider a spacetime consisting of three different regions with the internal and external ones reproducing a de-Sitter and a Schwarzschild spacetime at finite radii, r_1 and r_2, respectively. In addition, we follow the suggestion made in [10] and use a thick shell with a continuous profile of anisotropic pressures to avoid the introduction of infinitesimally thin shells of matter as demanded by the MM [1]. We start therefore with a metric of the form

$$\mathrm{d}s^2 = -\mathrm{e}^{\nu(r)}\mathrm{d}t^2 + \mathrm{e}^{\lambda(r)}\mathrm{d}r^2 + r^2\mathrm{d}\Omega^2\,, \tag{13}$$

and a fluid stress-energy tensor $T^\mu{}_\nu = \mathrm{diag}[-\rho, p_r, p_t, p_t]$, where p_r and p_t are the radial and tangential pressures, respectively. The Einstein field equations for this spacetime geometry

and matter distribution are

$$e^{-\lambda}\left(\frac{\lambda'}{r} - \frac{1}{r^2}\right) + \frac{1}{r^2} = 8\pi\rho\,, \tag{14}$$

$$e^{-\lambda}\left(\frac{\nu'}{r} + \frac{1}{r^2}\right) - \frac{1}{r^2} = 8\pi p_r\,, \tag{15}$$

$$e^{-\lambda}\left(\frac{\nu''}{2} - \frac{\lambda'\nu'}{4} + \frac{\nu'^2}{4} + \frac{\nu' - \lambda'}{2r}\right) = 8\pi p_t\,. \tag{16}$$

It is now convenient to transform the above equations into a form where the hydrodynamical properties of the system are more evident and that reduces to the TOV equations for systems with isotropic pressure, *i.e.*,

$$e^{-\lambda} = 1 - \frac{2m(r)}{r}\,, \tag{17}$$

$$\nu' = \frac{2m(r) + 8\pi r^3 p_r}{r(r - 2m(r))}\,, \tag{18}$$

$$p_r' = -(\rho + p_r)\frac{\nu'}{2} + \frac{2(p_t - p_r)}{r}\,, \tag{19}$$

where

$$m(r) \equiv \int_0^r 4\pi r^2 \rho \mathrm{d}r\,. \tag{20}$$

Combining (18) and (19), we obtain the anisotropic TOV equation

$$p_r' = -(\rho + p_r)\frac{m(r) + 4\pi r^3 p_r}{r(r - 2m(r))} + \frac{2(p_t - p_r)}{r}\,, \tag{21}$$

which is reminescent of the Newtonian hydrostatic-equilibrium equation and where the last term is obviously zero in the case of isotropic pressures, *i.e.*, $p_t = p_r$.

3.2. Equation of state

In order to adopt the model suggested in [10], and still maintain the simple structure of the MM model, we make the following choices for our density function $\rho(r)$

$$\rho(0) = \rho(r_1) = \rho_0, \qquad \rho(r_2) = 0\,, \qquad \rho'(r_1) = \rho'(r_2) = 0\,. \tag{22}$$

A simple way to satisfy the above conditions is to consider a cubic dependence in r,

$$\rho(r) = \begin{cases} \rho_0\,, & 0 \le r \le r_1 & \text{region I.} \\ ar^3 + br^2 + cr + d\,, & r_1 < r < r_2 & \text{region II.} \\ 0\,, & r_2 \le r & \text{region III.} \end{cases}, \tag{23}$$

with the coefficients a, b, c, d given by

$$a = \frac{2\rho_0}{(r_2 - r_1)^3}\,, \tag{24}$$

$$b = -\frac{3\rho_0(r_2 + r_1)}{(r_2 - r_1)^3}\,, \tag{25}$$

$$c = \frac{6\rho_0 r_1 r_2}{(r_2 - r_1)^3}\,, \tag{26}$$

$$d = \frac{\rho_0(r_2^3 - 3r_1 r_2^2)}{(r_2 - r_1)^3}\,. \tag{27}$$

To obtain the density in the terms of the total mass $m(r_2) = M$, we write

$$\rho_0 = M \frac{(r_2 - r_1)^3}{4\pi} \left[\frac{(r_2^6 - r_1^6)}{3} - \frac{3(r_2 + r_1)(r_2^5 - r_1^5)}{5} + \frac{3r_1 r_2(r_2^4 - r_1^4)}{2} + \right.$$
$$\left. + \frac{(r_2^3 - 3r_1 r_2^2)(r_2^3 - r_1^3)}{3} + \frac{r_1^3(r_2 - r_1)^3}{3} \right]^{-1}. \qquad (28)$$

For the radial pressure p_r, we follow the suggestion made in refs. [15, 11] and use an EOS of the type

$$p_r(\rho) = \left(\frac{\rho^2}{\rho_0} \right) \left[\alpha - (1 + \alpha) \left(\frac{\rho}{\rho_0} \right)^2 \right]. \qquad (29)$$

Clearly, the EOS (29) cannot be derived from basic principles and serves here essentially as a closure relation for the system of the equations. Yet, such an EOS can be constrained and the parameter α is determined by demanding that the maximum sound speed $\mathrm{d}^2 p_r/\mathrm{d}\rho^2 = 0$ coincides with the speed of light to rule out a superluminal behaviour. Because the sound speed

$$c_s \equiv \frac{\mathrm{d}p_r}{\mathrm{d}\rho} = 2 \left(\frac{\rho}{\rho_0} \right) \left[\alpha - 2(1 + \alpha) \left(\frac{\rho}{\rho_0} \right)^2 \right], \qquad (30)$$

has a maximum for $\bar\rho = \rho_0 \sqrt{\alpha/(2(1 + \alpha))}$, requiring $c_s(\bar\rho) = 1$ yields $\alpha \simeq 2.2135$. Despite being not particularly realistic, the EOS (29) has the advantage of being simple and of possessing the needed physical limits since $p_r \to -\rho$ for $r \to r_1$ and $p_r \to 0$ for $r \to r_2$ (*cf.* right panel of figure 2 for a typical gravastar model).
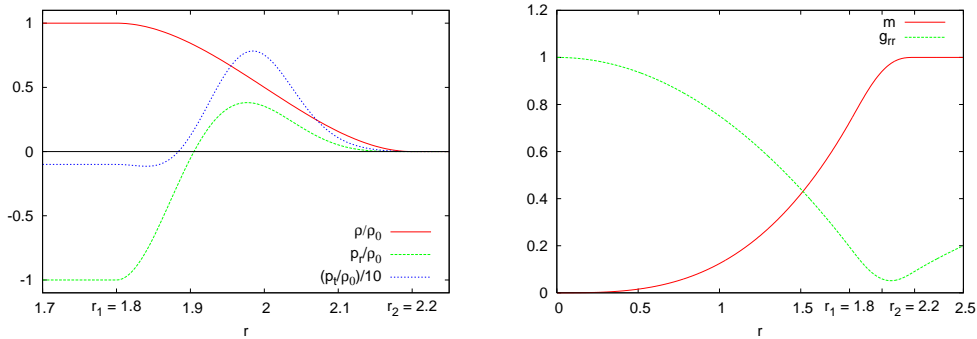

Figure 2. *Left panel:* Behaviour of the functions $\rho(r)$, $p_r(r)$ and $p_t(r)$ for a representative gravastar model with $M = 1$, $r_1 = 1.8$ and $r_2 = 2.2$. The function $p_t(r)$ is scaled by 0.1 for better visualization but provides the dominant contribution in eq. (21). *Right panel:* Behaviour of the mass function $m(r)$ and of the metric coefficient g_{rr} for the same solution shown in the left panel.

Once the solutions for the energy density and the radial pressure are known, the tangential pressure p_t can be computed through the anisotropic TOV equation (21) as

$$p_t = p_r + \frac{r}{2} p_r' + \frac{1}{2}(p_r + \rho) \left[\frac{m(r) + 4\pi r^3 p_r}{r(1 - 2m(r)/r)} \right]. \qquad (31)$$

The set of equations (22)–(31) fully determines our gravastar model which will have a finite core described by the de-Sitter metric, a crust of matter and an exterior described by the Schwarzschild solution.

   The behaviour of the energy density and of the pressures is shown in the left panel of figure 2 for a representative gravastar model with $M = 1$, $r_1 = 1.8\,M$ and $r_2 = 2.2\,M$. The right panel on the same figure, instead, shows the mass function and the metric coefficient g_{rr} for the same representative model.

3.3. Conditions on the metric functions

While equations (22)–(31) allow to construct gravastar models, additional constrains need to be imposed to guarantee that the metric functions g_{tt} and g_{rr} (and their first derivatives) have the expected properties once our choice for the EOS $p_r(\rho)$ and $\rho(r)$ is made. In particular, it is not difficult to conclude that $m(r)$ and $m'(r)$ are continuous for the choice of $\rho(r)$ made in equation (23), so that using equation (17) g_{rr} and its first derivative are continuous throughout the spacetime.

   Similar considerations apply for the metric function g_{tt}, for which we note that in obtaining the solution for ν by integrating equation (18) we must allow for a constant of integration ν_0 so that

$$\nu = \int_0^r \frac{2m(r) + 8\pi r^3 p_r}{r(r - 2m(r))} \mathrm{d}r + \nu_0 \,. \tag{32}$$

The integration constant can then be determined through the condition that, at the surface of the gravastar, $g_{tt}(r_2) = -(1 - 2M/r_2)$, thus giving

$$g_{tt} = -\mathrm{e}^{\nu(r)} = -\left(1 - \frac{2M}{r_2}\right) \mathrm{e}^{\Gamma(r) - \Gamma(r_2)} \,, \tag{33}$$

where

$$\Gamma(r) \equiv \int_0^r \frac{2m(r) + 8\pi r^3 p_r}{r(r - 2m(r))} \mathrm{d}r \,. \tag{34}$$

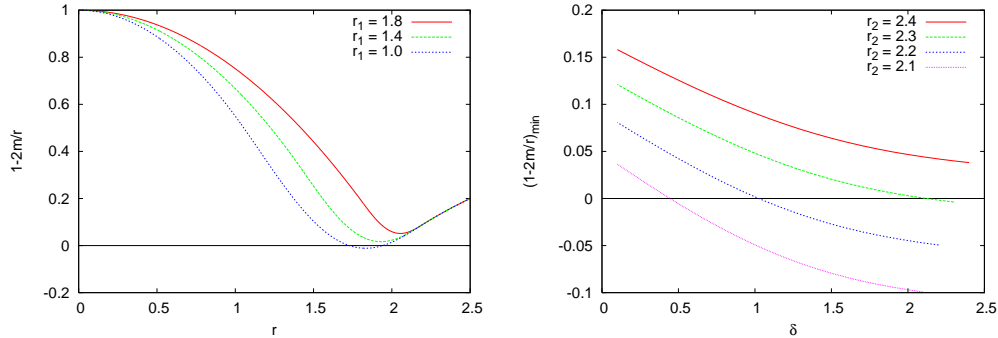In this way g_{tt} and g'_{tt} are continuous across r_2 and throughout the spacetime.

Figure 3. *Left panel:* Behaviour of $1 - 2m(r)/r$ for $M = 1$ and different values of r_1 and $r_2 = 2.2$. *Right panel:* Dependence on δ of the minimum value of $1 - 2m(r)/r$ for gravastars with $M = 1$ and different values of r_2. Note that for sufficiently large models, the minimum is always positive.

   The requirement for the metric functions of being continuous with continuous first derivatives is, in general, not sufficient to guarantee the existence of acceptable equilibrium models. The three free parameters M, r_1 and r_2, in fact, cannot be chosen arbitrarily but in such a way that g_{rr} is always positive. In the left panel of figure 3 we show a typical example

of the behaviour of the function $1 - 2m(r)/r$, where different lines refer to different values of the inner radius r_1 while the outer one r_2 is held fixed. Clearly, an incorrect choice of r_1 and r_2 leads to negative values for g_{rr} and thus to the unphysical appearance of horizons. The right panel of figure 3 shows how the minimum value of the function $1 - 2m(r)/r$ depends on the gravastar's thickness δ and that gravastars with large thicknesses can be built if the outer radius r_2 is chosen to be sufficiently large, that is, if the compactness μ is sufficiently small.

As a more systematic characterization of this problem, we have constructed a large number of gravastar models in which we have varied both the compactness μ and the thickness δ. In this way we can extend the diagram presented in figure 1 for the existence of MM models to our thick-shell gravastar model and define the region in the (δ, μ) parameter space where equilibrium solutions can be found. In particular, by defining the parameter ϵ as the dimensionless distance of the gravastar's surface from a Schwarzschild horizon, *i.e.*, $\epsilon \equiv r_2/M - 2$, we find that for $\epsilon > \epsilon_c \approx 0.3085$, the function $1 - 2m(r)/r$ is always positive, so that the thickness δ can be as large as r_2 (*i.e.*, r_1 can also be taken to be zero). On the other hand, for $\epsilon \leq \epsilon_c$ there exists a critical thickness $\delta_c = \delta_c(r_2, M)$ above which equilibrium models cannot be found because of the appearance of horizons. For $\epsilon = \epsilon_c$, we have found that $\delta_c = 2.30685\,M$.
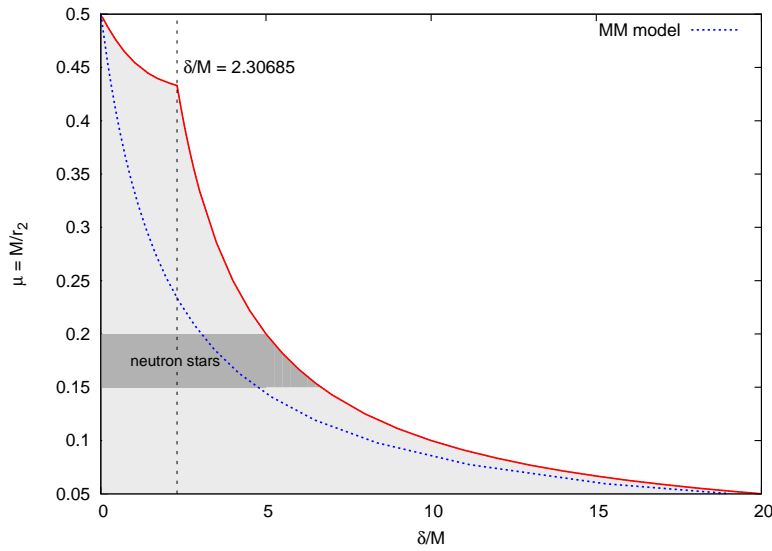

Figure 4. Limit on the compactness μ of the gravastar with the thickness of the shell δ. This figure compares the results obtained for the MM model in the lower curve (see figure 1) and the results obtained for our model in the upper curve.

Figure 4 summarizes these results by showing the region of the parameter space (δ, μ) where equilibrium models can be calculated. Equilibrium solutions for our model can be found in the region below the solid line, and $\delta/M = 2.30685$ is the boundary between the two distinct behaviors discussed above. Indicated with a dashed line is the corresponding threshold for the MM model (*cf.* figure 1). Overall, the data in the figure reveals that our thick-shell model obeys similar but less restrictive bounds than the MM model.

4. Perturbation equations and numerical methods

In order to assess the stability of gravastars against axial perturbations we have followed the standard procedure to study non-radial oscillations of stars [12, 13, 16, 17]. This approach differs from the one adopted in ref. [11], where the analysis of the axial perturbations of a gravastar was made following the standard procedure for Schwarzschild black holes (see [18] for a review) in order to study only the asymptotic properties of the potential and determine whether it has compact support and is everywhere positive.

We note that the pressure anisotropy in the shell does not play an important role in the study of axial tensor perturbations since these perturbations hardly excite fluid motions. As a result, the standard analysis for stars with isotropic pressures can be used here. This is no longer true for polar perturbations (for which the pressure anisotropy plays an important role) and a study on radial perturbations of stars with anisotropic pressures was recently presented in [19, 20].

As for Schwarschild black holes or spherical relativistic stars, the propagation of axial perturbations in the gravastar spacetime is governed by the wave equation in a scattering potential

$$\frac{\partial^2 \psi}{\partial r_*^2} - \frac{\partial^2 \psi}{\partial t^2} = V_\ell(r)\psi \,, \tag{35}$$

where the "tortoise" coordinate is here defined as

$$r_* \equiv \int_0^r e^{(\lambda - \nu)/2} dr \,, \tag{36}$$

and the scattering potential is given by the expression

$$V_\ell(r) \equiv \frac{e^\nu}{r^3} \left[\ell(\ell+1)r + 4\pi r^3(\rho - p_r) - 6m \right] \,. \tag{37}$$

The potential vanishes for $r \to \infty$ and diverges as $1/r^2$ for $r \to 0$, as a result of the centrifugal term proportional to $\ell(\ell+1)/r^2$. This is an important difference that the potential $V_\ell(r)$ has with respect to its counterpart for a Schwarzschild black hole, where $V_\ell(r) \to 0$ at the horizon $r = 2M$. Note also that $e^\nu \to 1$ for $r \to \infty$ (the spacetime is the Schwarzschild one for $r > r_2$) and, from eqs. (33) and (34), $e^\nu \to (1 - 2M/r_2)e^{-\Gamma(r_2)}$ for $r \to 0$.

Unlike for black-hole spacetimes, both the tortoise coordinate and the scattering potential are here not expressed through simple algebraic relations but need to be computed as solutions of ordinary differential equations. We have done so using a 4th order Runge-Kutta method to obtain e^ν and r_* from equations (33) and (36), respectively.

Introducing now the "light-cone" (null) variables $u \equiv t - r_*$ and $v \equiv t + r_*$, the wave equation (35) can be written in the more compact form as

$$-4\frac{\partial^2 \psi}{\partial u \partial v}(u, v) = V_\ell(r)\psi(u, v) \,, \tag{38}$$

and thus be integrated numerically. In particular, we have used a variation of the method used in [21] and in many other works, and derived a strict second-order accurate discretization given by

$$\psi_N = (\psi_E + \psi_W)\frac{16 - \Delta^2 V_S}{16 + \Delta^2 V_S} - \psi_S + \mathcal{O}(\Delta^4) \,, \tag{39}$$

where the indices N, S, E and W refer to the grid-points defined as $N \equiv (u + \Delta, v + \Delta)$, $S \equiv (u, v)$, $E \equiv (u, v + \Delta)$, and $W \equiv (u + \Delta, v)$. Equation (38) was then numerically integrated in the (u, v) plane with the algorithm (39) using a triangular grid limited by the

lines $r_* = r_*^{min}$ and $u = 0$, where r_*^{min} is a small value which we have set as $r_*^{min} = \Delta/2$. A schematic representation of the null grid is presented in fig. 5, where the black points represent the grid points where the solution is known, while the red ones are those where the solution is to be calculated.
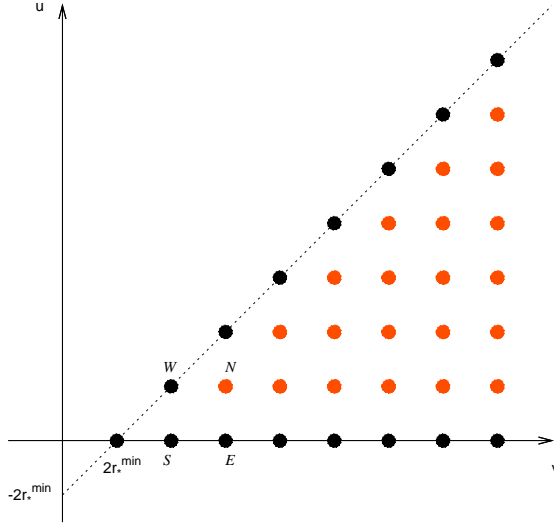
Figure 5. Diagram of the numerical grid and the domain of interest. The black points represent the grid points where the value of the field is known. The red points represent the grid points to be calculated.

In a linear regime the eigenfrequencies of the gravastar are not sensitive to the choice of the initial data and thus we have modelled the initial perturbation with the simplest possible choice, *i.e.* a Gaussian pulse centred around v_c and with witdth σ

$$\psi(u = u_0, v) = \exp\left[-\frac{(v - v_c)^2}{2\sigma^2}\right] , \tag{40}$$

where, to satisfy the regularity condition at the origin, we set

$$\psi(r_*^{min}, t) = \psi(u = v - v_0, v) = 0 , \qquad \forall t . \tag{41}$$

During the integration of eq. (38) we extract the values of the field ψ along a line of constant r_*, *i.e.*, at the points $(u = v - 2r_*, v)$. We let the field evolve for large values of t, until the transient is over and possible contributions of the higher overtones have died off. Only then, when the signal consists of the fundamental mode (the slowest decaying mode) and of its overtones, we can compute the real ω_R and imaginary part ω_I of its eigenfrequency with a least-squares fit of the function

$$\psi_{fit}(t) = A_n \exp(\omega_I^n t) \cos(\omega_R^n t + \phi) , \tag{42}$$

where A and ϕ are constant coefficients and n represents the order of the mode and this is not meant as an exponent. Once the properties of the fundamental mode are known, the eigenfrequencies of the overtones are obtained using the method proposed in [22], which consists of subtracting from the numerical solution the fitted function relative to the fundamental mode $n = 0$. This reveals the $n = 1$ mode and the procedure can be iterated for obtaining higher overtones, depending on their damping rate. Of course, very rapidly

decaying modes cannot be obtained by this procedure, but this approach is a very efficient and easy way to obtain the first overtones in a signal, which are the ones expected to be detected from any astrophysical sources.

The numerical setup described above has been first tested by performing a perturbation analysis of Schwarzschild stars, *i.e.*, uniform-density spherical stars, obtaining results that are in very good agreement with the values reported in the literature [13, 23].

5. Results

Before discussing the results of the perturbative analysis, we note that the axial potential given in (37) shows features which are similar to those that are well-known in compact uniform-density stars [13]. Quite generically, in fact, the potential exhibits at least a minimum and a maximum, thus indicating the possibility of having modes that are trapped in the potential well.

In figure 6 we present some typical examples of the scattering potential $V_\ell(r)$ when $\ell = 2$ and which, in general, depends on both the compactness μ (as for relativistic stars) and on the thickness of the shell δ. The left panel of figure 6, in particular, shows the potential of gravastar models having the same compactness $\mu = 0.46$ but increasing thickness of the shell, while the right panel reports how the potential changes for gravastar models with the same shell-thickness $\delta = 0.2$ but increasing compactness. Clearly, in the exterior region $V_\ell(r)$ is just the Schwarzschild potential for axial perturbations and the depth of the potential well in the interior region increases with both μ and δ. Furthermore, given the chosen EOS (29), it is also possible to select the parameters r_1, r_2, and M such that $V_\ell(r)$ has two local minima very close to each other. This is shown by the curve with $\mu = 0.35$ in the right panel of figure 6.
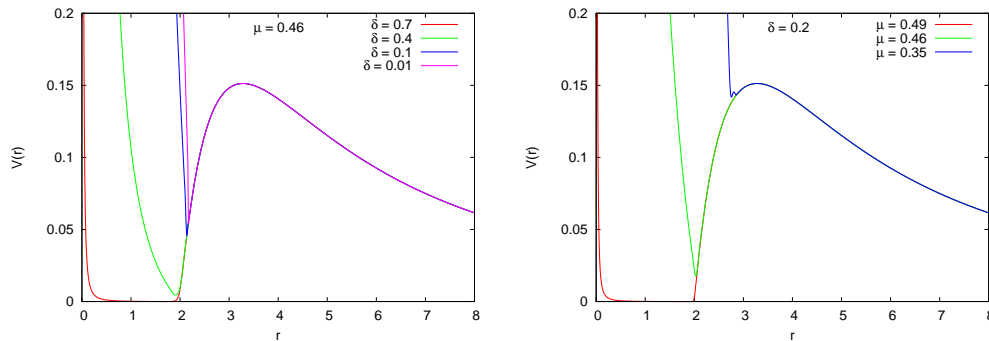

Figure 6. *Left panel:* The scattering potential $V_\ell(r)$ with $\ell = 2$ of gravastar models with the same compactness $\mu = 0.46$ but increasing thickness of the shell. *Right panel:* The same as in the left panel but gravastar models with the same shell-thickness $\delta = 0.2$ but increasing compactness.

Following the procedure outlined in the previous Section, we have integrated the perturbation equation (38) for a large variety of gravastar models differing in mass, compactness and thickness. Figure 7 reports some typical results and shows the time evolution of the perturbations for a representative gravastar with $M = 1$, and radii $r_1 = 1.96$, $r_2 = 2.26$. The left panel, in particular, reports the total solution $\psi(t)$ as extracted at $r_* = 10$ during the initial stages of the scattering off the potential and allows one to discern the "beating" caused by the superposition of overtones and other rapidly decaying components of the signal. Interestingly, this beating of the fundamental mode with overtones becomes more pronounced

Table 1. Some typical values obtained for the the first overtones of the gravastars QNM eigenfrequencies for axial perturbations with $\ell = 2$. The gravastars have $M = 1$, $r_2 = 2.26$ and δ given in the Table. We also show for comparison the equivalent frequencies for a Schwarzschild black hole of the same mass and for a standard TOV star with uniform density with $M = 1$ and $R = 2.26M$ (note that for these stars one must have $R/M > 2.25$ [13]).

	$n = 0$		$n = 1$		$n = 2$	
model	ω_R	$-\omega_I$	ω_R	$-\omega_I$	ω_R	$-\omega_I$
$\delta = 0.30$	0.3281	2.481e-3	0.4865	6.264e-2	0.6534	1.590e-1
$\delta = 0.35$	0.2943	7.081e-4	0.4459	3.202e-2	0.5922	1.093e-1
$\delta = 0.40$	0.2575	1.543e-4	0.4011	1.227e-2	0.5384	5.814e-2
Schwarzchild black hole	0.3737	8.896e-2	0.3467	2.739e-1	0.3011	4.783e-1
Schwarzchild star	0.1090	1.239e-9	0.1484	3.950e-8	0.1876	5.470e-7

with increasing μ and δ, underlining that the contribution of the overtones increases (*i.e.*, the modes decay more slowly) with both μ and δ (*i.e.*, as the the depth of the potential well increases). A similar relation between the decay rate of the modes and the potential well is known for the "trapped modes" of compact uniform-density stars [23].
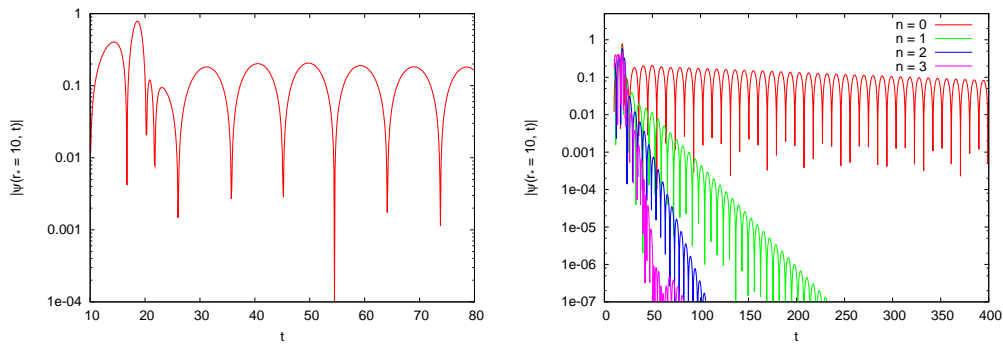

Figure 7. *Left panel:* Evolution of the axial perturbations $\psi(t)$ as extracted at $r_* = 10$ and during the initial stages of the scattering for a gravastar with $M = 1$, $r_1 = 1.96$ and $r_2 = 2.26$. *Right panel:* The same as in the left panel but when the contribution of the fundamental mode $n = 0$, is distinguished from that of the overtones $n = 1, 2$ and 3.

The right panel of figure 7, on the other hand, shows the evolution of the perturbations over a longer timescale and when the overtones have been "removed" from the general signal using the approach discussed in the previous Section. Note that, for increasing n, the period of the oscillations becomes smaller, and the decaying timescale shorter. Using a least-squares fit of the numerical data to the *ansatz* (42) we have computed the real and imaginary parts of the QNM eigenfrequencies and the numerical results for some typical cases are presented in table 1, where they are also compared to the corresponding values for a Schwarzschild black hole of the same mass and a Schwarzschild star of the same compactness. The tabulated values are all for an $\ell = 2$ perturbation and refer to the fundamental mode and to the first two overtones since the third one does not usually have a sufficiently clear slope to allow for an accurate measurement. If necessary, an increase in spatial resolution would improve the decay of higher overtones and allow for their computation.

Figure 8 is the most important of this paper and it reports the variation of the $\ell = 2$, $n = 0$

QNM eigenfrequencies as a function of the parameters of the gravastar: μ and δ. The two panels report separately the behaviour of the real and imaginary parts and indicate that both the period of the oscillations $\tau_R \equiv 2\pi/\omega_R$ and the the damping time $\tau_I \equiv 2\pi/|\omega_I|$ increase with increasing δ and μ. The two thick horizontal lines represent instead the corresponding frequencies for a Schwarzschild black hole of the same mass, *i.e.*, $M\omega_R = 0.37367$ and $M\omega_I = -0.08896$ [16]. Clearly, while it is always possible to select the thickness and compactness of the gravastar such that it will have the same oscillation frequency of a black hole with the same mass (*cf.*, left panel), the corresponding decaying time will be different and about one order of magnitude larger (*cf.*, right panel). Stated differently, a gravastar and a black hole with the same mass cannot have the same complex QNM eigenfrequency when subject to axial perturbations. This result, which we have here presented for the fundamental mode, can be shown to be true also for the first two overtones.
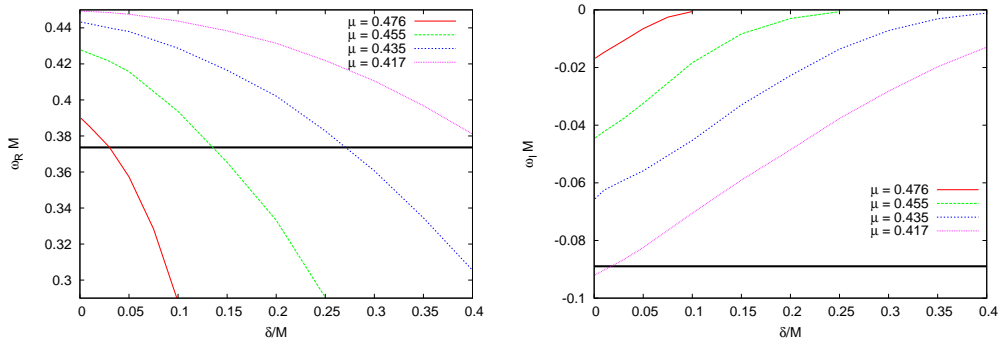

Figure 8. *Left panel:* Behaviour of the real part ω_R of the $\ell = 2$, $n = 0$ QNM eigenfrequencies as functions of δ for different values of μ. *Right panel:* The same as in the left panel but for the imaginary part ω_I of the eigenfrequencies. In both panels, the thick horizontal lines represent the corresponding frequencies for a Schwarzschild black hole.

6. Conclusions

Although the gravastar model of Mazur and Mottola [1] represents an ingenious solution of the Einstein equations in spherical symmetry, it has also challenged one of the most cherished foundations of modern astrophysics: *i.e.,* the existence of astrophysical black holes. Gravastars, in fact, can be constructed to be arbitrarily compact, with an external surface which is only infinitesimally larger than the horizon of a black hole with the same mass. As a result, the electromagnetic emission from the surface of a gravastar will suffer of essentially the same gravitational redshift as that of a black hole, thus making it difficult, if possible at all, to distinguish the two when only electromagnetic radiation is available.

Without entering the relevant debate about the physical processes that would lead to the formation of a gravastar or the astronomical evidence in support of their existence [24], we have here considered two more fundamental questions: Is a gravastar *stable* against generic perturbations? If so, can an external observer *distinguish* it from a black hole? The short answers to these questions are that: a gravastar *is stable* to axial perturbations and indeed *it is possible* to distinguish it from a black hole if gravitational radiation is produced.

To reach the first of these conclusions we have constructed a general class of gravastar models that extends the one proposed by Mazur and Mottola by replacing the infinitesimal shell of matter with one having finite size δ and variable compactness μ. These

equilibrium solutions of the Einstein equations have then been analyzed when subject to axial perturbations and the eigenfrequencies of the corresponding QNMs have been computed explicitely. For all of the cases considered, the imaginary part of the eigenfrequencies has always been found to be negative, thus indicating the stability of these objects with respect to this type of perturbations.

To reach the second conclusion, instead, we have shown that the QNM spectra of a gravastar and that of a black hole of the same mass differ considerably. In particular, while it is always possible to select δ and μ such that the gravastar has the same oscillation frequency as that of a black hole with the same mass, the corresponding decaying time will be different. As a result, the gravitational radiation produced by an oscillating gravastar can be used to distinguish it, beyond dispute, from a black hole of the same mass.

We plan to extend our stability analysis also to polar perturbations and determine whether or not these intriguing objects possess modes of oscillation that do not have a counterpart in compact relativistic stars and may therefore hint to new solutions of the Einstein equations.

Acknowledgments

References

[1] Mazur P O and Mottola E 2001 Gravitational condensate stars: an alternative to black holes
[2] Chapline G 2004 Dark energy stars *Proceedings of the 22nd Texas Conference on Relativistic Astrophysics (California)*
 Mazur P O and Mottola E 2004 Gravitational vacuum condensate stars *Proc.Nat.Acad.Sci.* **111** 9545-50
[3] Israel W 1966 Singular hypersurfaces and thin shells in general relativity *Nuovo Cimento* **B44** 1-14
 Israel W 1967 Erratum *Nuovo Cimento* **B48** 463
 Misner C W, Thorne K S and Wheeler J A 1997 *Gravitation* (New York: W. H. Freeman and Company) p 505-16, 551-6
[4] Abramowicz M A, Kluzniak W and Lasota J P 2002 No observational proof of the black-hole event-horizon *Astron. Astrophys.* **396** L31-4
[5] Visser M and Wiltshire D L 2004 Stable gravastars - an alternative to black holes? *Class. Quant. Grav.* **21** 1135-51
[6] Carter B M N 2005 Stable gravastars with generalised exteriors *Class. Quant. Grav.* **22** 4551-62
[7] Bilić N, Tupper G B and Viollier R D 2006 Born-Infeld phantom gravastars *JCAP* 2-13
[8] Lobo F S N 2006 Stable dark energy stars *Class. Quant. Grav.* **23** 1525-41
[9] Lobo F S N and Arellano A V B 2007 Gravastars supported by nonlinear electrodynamics *Class. Quant. Grav.* **24** 1069-88
[10] Cattoen C, Faber T and Visser M 2005 Gravastars must have anisotropic pressures *Class. Quant. Grav.* **22** 4189-202
[11] DeBenedictis A, Horvat D, Ilijic S, Kloster S and Viswanathan K S 2006 Gravastar solutions with continuous pressures and equation of state *Class. Quant. Grav.* **23** 2303-16
[12] Chandrasekhar S and Ferrari V 1991 On the non-radial oscillations of a star *Proc. R. Soc. Lond.* **A432** 247-79
[13] Chandrasekhar S and Ferrari V 1991 On the non-radial oscillations of a star III. A reconsideration of the axial modes *Proc. R. Soc. Lond.* **A434** 449-57
[14] Dymnikova I 1992 Vacuum nonsingular black hole *Gen. Rel. Grav.* **24** 235-42
 Dymnikova I and Galaktionov E (2005) Stability of a vacuum nonsingular black hole *Class. Quant. Grav.* **22** 2331-57
[15] Mbonye M R and Kazanas D 2005 A non-singular black hole model as a possible end-product of gravitational collapse *Phys. Rev.* D **72** 024616-23
[16] Kokkotas K D and Schmidt B G 1999 Quasi-normal modes of stars and black holes *Living Rev. in Relativity* **2** 2

[17] Nollert H 1999 Quasinormal Modes: The characteristic 'sound' of black holes and neutron stars *Class. Quantum Grav.* **16** R159-R216

[18] Nagar A and Rezzolla L 2005 Gauge-invariant non-spherical perturbations of Schwarzschild black-hole spacetimes, *Class. Quantum Grav.* **22**, R167-R192; erratum-ibid. **23**, 4297 (2006)

[19] Dev K and Gleiser M 2002 Anisotropic stars: Exact solutions *Gen. Rel. Grav.* **34** 1793-818

[20] Dev K and Gleiser M 2003 Anisotropic stars. 2. Stability *Gen. Rel. Grav.* **35** 1435-57

[21] Abdalla E, Chirenti C B M H and Saa A 2006 Quasinormal modes for the Vaidya metric *Phys. Rev.* D **74** 084029-34

[22] Abdalla E and Giugno D 2006 An extensive search for overtones in Schwarzschild black holes *Preprint* gr-qc/0611023

[23] Kokkotas K D 1994 Axial modes for relativistic stars *Mon. Not. R. Astron. Soc.* **268** 1015-8
Kokkotas K D 1995 Erratum: axial modes for relativistic stars *Mon. Not. R. Astron. Soc.* **277** 277
Abdalla E and Giugno D 2006 Shedding some new lights upon the stellar quasi-normal modes *Preprint* gr-qc/0612183

[24] Broderick A E and Narayan R 2007 Where are all the gravastars? Limits upon the gravastar model from accreting black holes *Class. Quant. Grav.* **24** 659-66